Millimeter-wave low profile continuous transverse stub arrays with novel linear source generators

Lu, Yunlong; You, Qingchun; Wang, Yi; You, Yang; Huang, Jifu; Wu, Ke

Millimeter-Wave Low Profile Continuous Transverse Stub Arrays With Novel Linear Source Generators

Yunlong Lu, Qingchun You, Yi Wang, *Senior Member, IEEE*, Yang You, Jifu Huang, and Ke Wu, *Fellow, IEEE*

Abstract—**This paper presents a new type of continuous transverse stub (CTS) antenna array with a novel linear source generator (LSG). The conventional multi-layer parallel-plate waveguide (PPW) feed and pillbox structure are eliminated and replaced with a more compact partially-corporate feed network. This helps to achieve a lower profile (or reduction of antenna layers) and high performance of broadband and high efficiency. For validation, two prototypes are demonstrated – one based on hollow waveguides operating at 34 – 41 GHz (Array-I) and the other based on substrate integrated waveguides (SIWs) operating at 24.5 – 29.5 GHz (Array-II). Both arrays contain eight radiation slots, fed from a single-layer PPW junction. The required quasi-TEM wave excitations are achieved by using the novel LSG of a jagged cavity structure. Detailed design methodology and analyses are provided in the paper. Measurements show that antenna efficiencies of over 83% and 82% with the peak gains of better than 27.6 dBi and 20.6 dBi are achieved for Array-I and II, respectively. These low-profile CTS designs are well suited for current and emerging millimeter-wave applications such as 5G and point-to-point communications.**

Keywords— ***Continuous transverse stub array, millimeter wave antennas, slot arrays, waveguide arrays.***

I. INTRODUCTION

The increasingly high data rates demand the wider use of millimeter-wave (MMW) spectrum in the current and emerging landscape of wireless communications [1]. Various high-gain antennas in millimeter-wave bands have been studied and demonstrated over recent years. These include reflector antennas [2], lens antennas [3], [4] and waveguide slot arrays [5], [6].

Y. Lu is with the Faculty of Electrical Engineering and Computer Science, Ningbo University, Ningbo 315211, China, and also with the State Key Laboratory of Millimeter Waves, Southeast University, Nanjing 210096, China.

Q. You, Y. You and J. Huang are with the Faculty of Electrical Engineering and Computer Science, Ningbo University, Ningbo, Zhejiang, 315211, China (e-mail: yqch2017@163.com).

Y. Wang is with School of Engineering, University of Birmingham, B15 2TT, United Kingdom (e-mail: y.wang.1@bham.ac.uk).

K. Wu is with the Faculty of Electrical Engineering and Computer Science, Ningbo University, Ningbo 315211, China, on leave from the Department of Electrical Engineering, Poly-Grames Research Center, Ecole Polytechnique de Montréal, University of Montreal, Montreal, QC H3T 1J4, Canada.

The reflector and lens antennas suffer from relatively large size and are often unacceptable for small form-factor wireless communication systems, where planar antenna arrays with a low profile are highly desired. Planar patch arrays [7]-[9] are the most common choice, but their feeding networks become cumbersome and lossy for highly directive arrays, leading to relatively low overall efficiency [10], [11]. This issue becomes more pronounced at millimeter-wave frequencies, when the material losses increase and transmission lines get narrower. Compared with planar transmission lines, waveguides have much lower losses. Slotted waveguide arrays have been a popular choice for high performance MMW antennas. However, they commonly suffer from narrow bandwidth and complex corporate-feed networks [12]-[14].

Continuous transverse stub (CTS) antenna arrays, for their high performance, have been considered a competitive candidate for advanced antenna systems [15]-[19]. A CTS antenna usually consists of a one-dimensional slot array and open-ended parallel-plate-waveguides (PPWs) feeding the array either in series or parallel. The parallel feeding structure is usually preferred for its broadband performance. The PPW is designed to support selectively the fundamental transverse electromagnetic (TEM) mode. Different types of CTS antenna arrays have been recently investigated. A Ka-band full-metal 16-slot CTS antenna fed by a pillbox-based linear source with a four-layer PPW network was reported in [20]. The antenna achieved a gain of over 27.6 dBi over a 12% bandwidth from 27.5 to 31 GHz. [21] presented a high-gain and broadband 32-slot CTS array excited in parallel by a uniform five-layer corporate PPW network combined with a pillbox coupler similar to [20]. Low temperature co-fired ceramic (LTCC) technology was also used for a CTS antenna in V-band [22]. Due to the restrictive thickness of the substrate layers in LTCC, only a small number of radiating slots were realized and the maximum radiation efficiency was just 44%. Like [22], most of the CTS arrays adopted a vertically cascaded power division network, the so-called multi-layer PPW feeding network. Further combined with a pillbox coupler, the whole antenna structure became bulky with a high profile. In addition, due to the non-uniform amplitude distribution of quasi-TEM wave generated by the pillbox coupler and PPW network, conventional CTS antenna arrays have a relatively low aperture efficiency [15]-[22]. All becomes more challenging at MMW frequencies due to the exacerbating issues with tolerance and reliability in the fabrication and assembly.

This work aims to address the abovementioned issues of antenna profile and low efficiency while taking advantage of the high performance of CTS antenna arrays. We propose a novel linear source generator (LSG) to replace the pillbox coupler in conventional CTS arrays. This is the main novelty of this work. The key features of the LSG include: (i) Compared with the pillbox coupler, the new LSG generates better quality quasi-TEM wave to excite a more uniform amplitude distribution along the radiation slot. This leads to higher aperture efficiency; (ii) By employing multiple LSGs in the same layer, the conventional multi-layer PPW network has been simplified into a single-layer PPW junction. Consequently, the profile (or the number of layers) of the CTS array is reduced effectively. The low-profile of the array has been further ensured by a horizontally expandable feeding network. Very recently, [23] reported an LSG in a beam steering design, providing a serial feed to the radiation slots. Our design is primarily for a fixed beam antenna array. We take advantage of the parallel feed with multiple LSGs to improve the operating bandwidth and reduce antenna profile. It is worth mentioning that the pillbox-coupler based CTS antenna has the advantage of facilitating beam steering. We are working on a beam steering design with the LSG structure in a future publication.

This paper will demonstrate two porotypes to verify the design concept. One uses hollow waveguide technology (Array-I), and the other is based on substrate integrated waveguide (SIW) (Array-II). We should mention that the architecture of Array-I was first reported briefly in [24]. Here we will provide detailed design of the constituent components, which contain the main innovation of the work. We will report comprehensively the performance of the components as well as that of the whole antenna in both simulations and measurements, which was absent from [24]. The main design drive for Array-II is to use a small number of substrate layers to realize a low-profile and high performance array that is easy to fabricate. The paper is organized as follows: Section II describes the novel LSG structure adopted in both prototypes. The design and analysis of Array-I and II are presented in Section III and IV, respectively. Conclusions are drawn in Section V.

II. PRINCIPLE OF THE LSG

A novel linear source generator is proposed in this work to replace the pillbox commonly used in conventional CTS arrays [19]-[22]. The LSG is a device used to convert the TE_{10} mode from the rectangular waveguide to a quasi-TEM wave with uniform amplitude and phase distributions, as required to excite the long radiation slots in a CTS antenna. The long LSG structure can be formed of multiple periodic units cascaded in line. Fig. 1(a) shows such a unit in hollow waveguide. It is segmented into four sections denoted as 1, 2, 1' and 2', each with a coupling slot. In simulation, periodic boundary condition is used on this unit. The TE_{10} mode from the input aperture propagates through the T-junction in the rectangular waveguide cavity. The coupling slots are alternated to tap to the propagating TE mode in phase. The unit length l_u (marked out in Fig. 1) is about $2 \times \lambda_{gmin}$ (λ_{gmin} is the minimum guided wavelength over the operating band in the cavity) to make sure

no grating lobes appear over the entire bandwidth. However, this configuration with staggering slots does not fit with the PPW structure that the LSG feeds into, which has a uniform waveguide structure. So, instead of staggering the coupling slots, they are streamlined into a long continuous slot whereas the rectangular waveguide sections are staggered into jagged cavities, resulting in the design adopted in this work, as illustrated in Fig. 1(b).
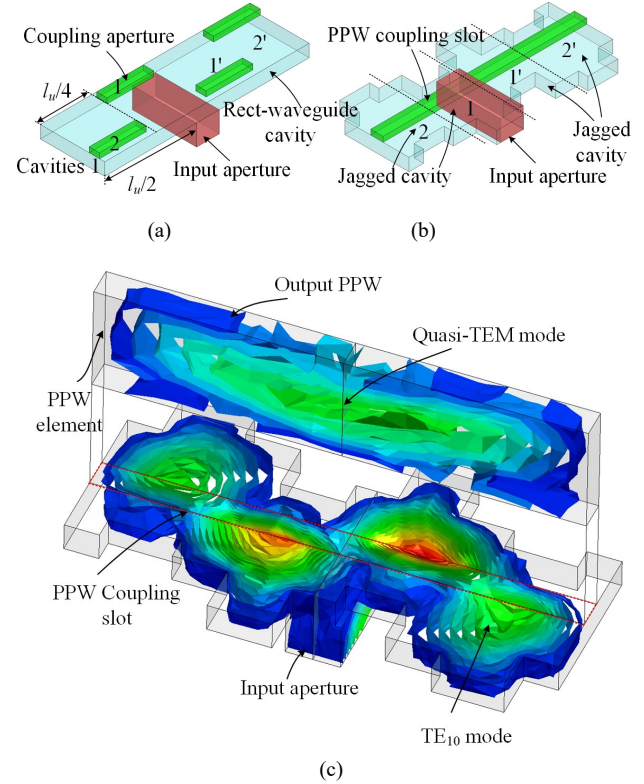
Fig. 1. (a) Schematic diagram of a LSG unit; (b) Proposed LSG unit; (c) Simulated filed distributions in the LSG unit and PPW element at the center frequency of the operating band.

Fig. 1(c) shows the E-field distributions in the LSG unit and the PPW element it feeds into. It can be seen that the TE_{10} wave from the input aperture is split into two paths to excite the jagged cavities 1 (1') and 2 (2') in series. They are then combined into a quasi-TEM wave in the PPW element. In this case, the jagged cavities in series and the coupling from the cavities to the PPW together function as a partially-corporate feed structure [26]. A significant benefit of this partially-corporate feed is that it halves the feed points of the LSG and simplifies the feeding network. However, it leads to phase imbalance between the adjacent LSG units. Therefore, phase compensation is required. There are two ways to do this. One is to add phase compensation structures, whereas the other is to replace the partial-corporate feed with a full-corporate feed. These two approaches will be demonstrated by Array-I and II, respectively. Details are given in Section III and IV.

III. DESIGN AND ANALYSIS OF ARRAY-I

This section presents Array-I, a hollow-waveguide CTS antenna array. The concerned frequency band is 34 - 41 GHz

and the center frequency f_{c1} is 37 GHz. All the simulations are performed using Ansoft HFSS.

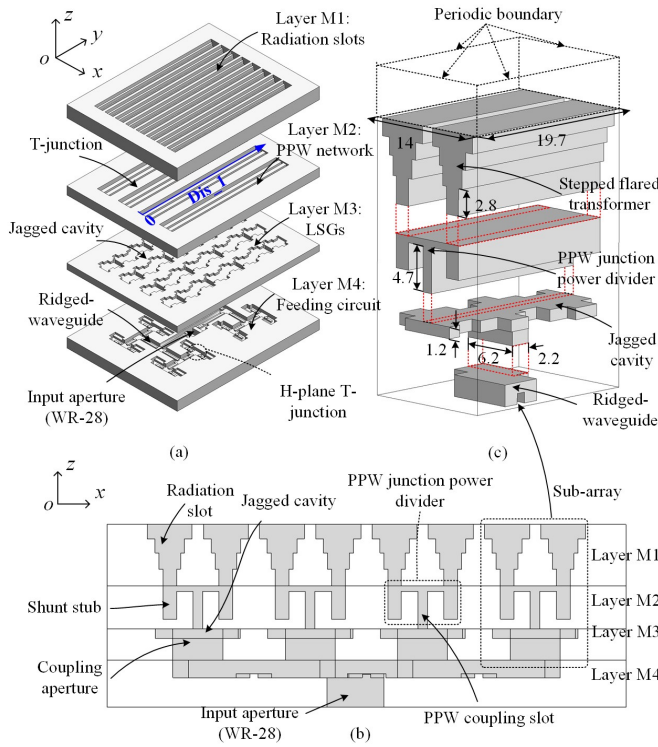Fig. 2. Array-I: (a) 3-D overview; (b) Cross-sectional view; (c) Sub-array. It should be noted that, for clarity, the 'air cavities' are shown in grey in (b) and (c). All dimensions are given in millimeters.

A. Antenna configuration

Array-I in its entirety and the sub-array as the building block are shown in Fig. 2. From Fig. 2(a), the CTS antenna array consists of four layers. The feeding circuit is in Layer M4 and the radiation part in Layers M1-M3. The feeding circuit contains a 16-way T-junction power divider based on H-plane ridged-waveguides. Its input port is a Ka-band standard waveguide at the center of the backside. The radiating part includes four LSGs in Layer M3, one single-layer PPW junction in Layer M2 and the radiation slots in Layer M1. The radiation slots are shorted at both ends. The operation principle of Array-I is summarized as follows:

1. The signal from the standard input waveguide is divided by the 1-to-16 ridged-waveguide power divider. The number of the divisions is determined by the number (eight in this case) and length of the radiation slots.
2. The 16 outputs from the power divider feed to the four rows of LSGs in Layer M3. Each row contains 4 units of jagged cavities shown in Fig. 1. The LSGs generate quasi-TEM wave to excite the radiation slots via the PPW network, as illustrated in Fig. 2(b).
3. The four rows of LSGs couple to the four rows of PPWs in Layer M2. Each PPW splits via a PPW junction power divider to excite two radiation slots.
4. Finally, the quasi-TEM waves radiate into free space from the radiation slots in Layer M1.

Now the radiation slots, PPW junction, LSG and the feeding

circuit will be discussed in more details. To simplify the analysis and simulation, the CTS array structure contained within Layer M1 to M3 is decomposed into a sub-array by setting periodic boundary conditions, as shown in Fig. 2(c). In this sub-array, the input is a ridge-waveguide taken from the output of the 16-way power divider in Layer M4.

B. PPW Junction Power Dividers and Radiation Slots

As mentioned in Section III-A, the array has four PPW junction power dividers in Layer M2, as shown in Fig. 2. Each feeds into a pair of slots. Here we consider equal power dividers, leading to a uniform power distribution among the radiation slots. Fig. 3(a) shows a pair of radiation slots and their matching sections, as seen in the E-plane. The stepped and flared impedance transformers have been used to match the output of the PPW junction power divider to free space. The design procedure was adopted from [20]-[22], [25].
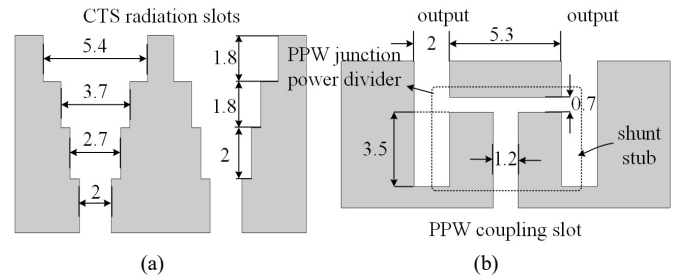
Fig. 3. E-plane cross-sectional view of: (a) the radiation slots; (b) the PPW junction power divider and shunt stubs in parallel with the feedlines. All dimensions are given in millimeters.
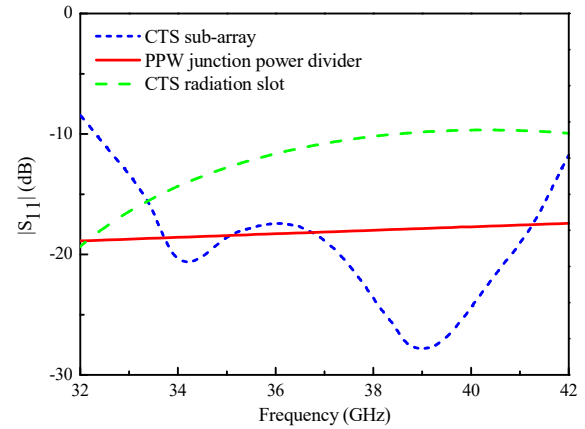
Fig. 4. Simulated reflection coefficient of the sub-array in Fig. 2(c), the PPW junction power divider and the radiation slot shown in Fig. 3.

Fig. 3(b) shows the PPW junction power divider. It is an E-plane T-junction, consisting of two half-height waveguides and a full-height waveguide. The shunt stubs in parallel are primarily employed to reduce the reactive impedances of the PPW junction and improve impedance matching. Later in the discussion about Fig. 7, it will also be shown to be effective in balancing the phases of the excitation signals at the radiation slots. The simulated reflection coefficients of the optimized radiation slot, the PPW junction and the sub-array are all shown

in Fig. 4. An impedance matching level of better than -17 dB (for the sub-array) over the entire operation bandwidth has been achieved. The dimensions of the PPW junction and the slots are provided in Fig. 2(c) and 3.

Fig. 5. Dimensions of the LSG unit. All dimensions are given in millimeters.

C. Linear source generator (LSG)

Four LSG units shown in Fig. 1 form one row of the LSG in Array-I. l_u is chosen to be $1.9 \times \lambda_{gmin}$ in this prototype. The dimensions of the optimized LSG unit are given in Fig. 5. The total length of the radiation slot is $4 \times l_u$, which is $7.6 \times \lambda_{gmin}$ (78.8 mm). To obtain a high qua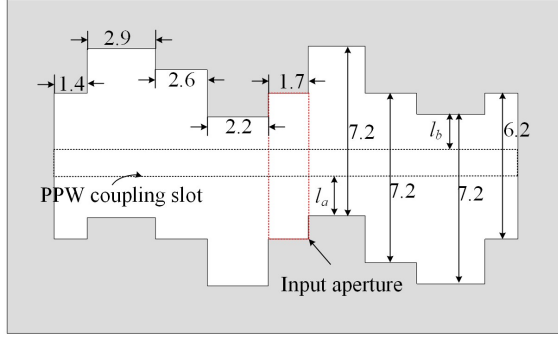lity of quasi-TEM wave from the LSG, the jagged cavities are firstly optimized with an objective to minimize the amplitude fluctuation of the E-field in the PPW element. This is done by adjusting l_a and l_b as marked out in Fig. 5. The simulated E-field amplitude differences between the adjacent jagged cavities as a function of l_a and l_b are shown in Fig. 6. A minimum amplitude fluctuation is obtained when l_a = 1.7 mm and l_b = 1.1 mm.
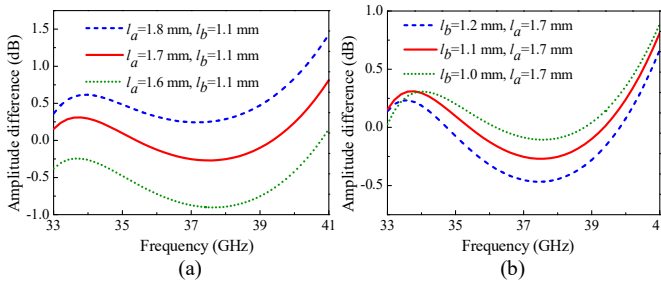

Fig. 6. Simulated E-field amplitude fluctuation between the adjacent jagged cavities as a function of: (a) l_a when l_b is 1.1 mm; (b) l_b when l_a is 1.7 mm.

A phase imbalance between the adjacent cavities could also exist. Without disturbing the amplitude balance achieved by the jagged cavities, the shunt stubs loaded to the PPW junction (Fig. 3(b)) are optimized to compensate for the phase imbalance (as well as ensuring impedance matching). This is evidenced by the comparison between Fig. 7(a) and (b) for the phase and amplitude variations along the *y*-axis of the PPW (see Fig. 2 for the coordinates). It is important to note that the improvement on the phase distribution with the shunt stubs in turn reduces the amplitude fluctuation further. Without the shunt stubs, an amplitude imbalance of more than 8.5 dB occurs due to the larger phase fluctuation. By using the shunt stubs, the phase imbalance is reduced to within 9.8°, and thus the amplitude fluctuation is reduced to 3.5 dB. The side lobes are also suppressed as a result of the well-distributed amplitude, as

shown in the comparison of radiation pattern before and after introducing the shunt stubs in Fig. 7(c) and (d).
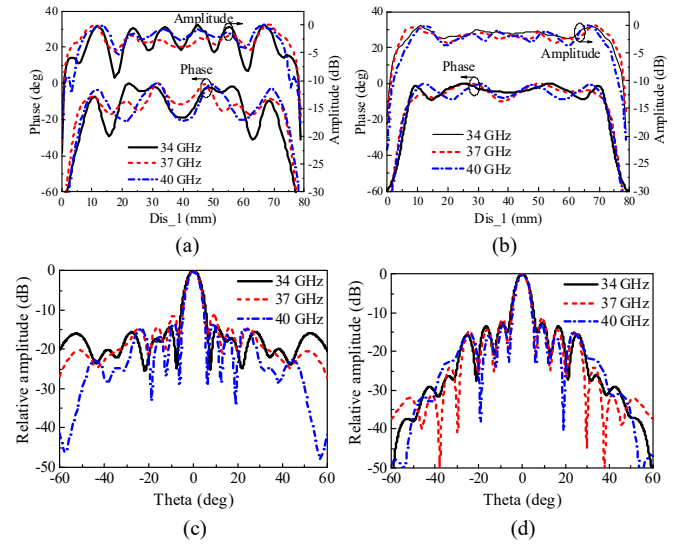
Fig. 7. (a) E-field amplitude and phase distributions without shunt stub; (b) E-field amplitude and phase distributions with shunt stub; (c) H-plane radiation patterns without shunt stub; (d) H-plane radiation patterns with shunt stub.
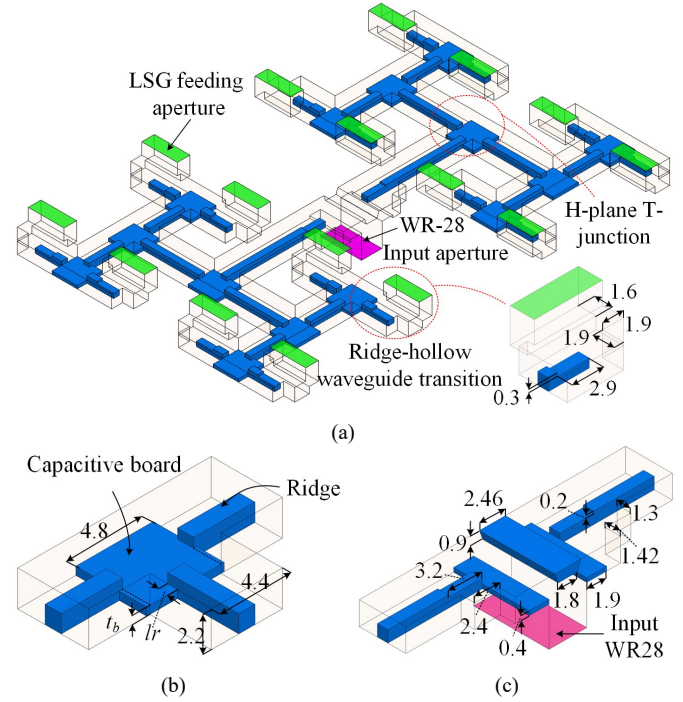
Fig. 8. (a) The 16-way ridged waveguide power divider. (b) The H-Plane T-junction. (c) E-Plane T-junction with standard input WR28. All dimensions are given in millimeters.

D. Feeding Circuit

There are four rows of LSGs, each requiring four excitation apertures. So the feeding circuit is designed to divide the TE_{10} wave from the standard waveguide port (WR28) into 16 ways to excite the 16 LSG units. Fig. 8(a) shows the power divider built on hollow- and ridge-waveguides. The latter are employed to ensure compactness. It has one E-plane T-junction at the center and fourteen cascaded H-plane T-junctions. Transitions

are implemented to convert the ridge waveguides to hollow rectangular waveguides at the 16 output ports. The E- and H-plane T-junctions are shown in Fig. 8(b) and (c) respectively. A capacitive board is embedded in each of the H-plane T-junction to increase bandwidth, as shown in Fig. 8(b). The impedance matching can be controlled by the height of the board (t_b) and the overlapping length (l_r) between the capacitive board and ridge. The parameter studies of this junction can be found in Fig. 9. When $t_b = 0.45$ mm and $l_r = 1.6$ mm, reflection coefficient lower than -20 dB can be achieved over the bandwidth of 26 - 47 GHz.

Fig. 9. Impedance matching analysis of the H-plane T-junction as shown in Fig. 8(b): (a) different values of l_r, (b) different values of t_b.

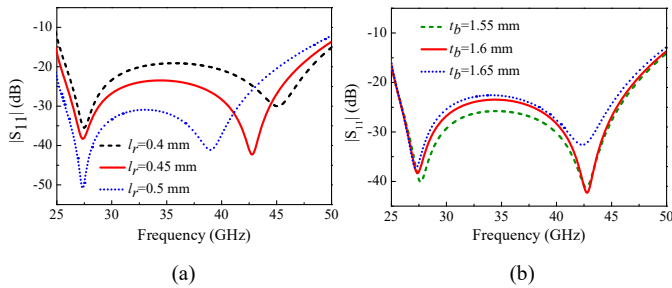For the E-plane T-junction in Fig. 8(c), two three-section impedance transformers are used to match the ridge-waveguide at its output ports. In addition, two-section impedance transformers and ridge-to-hollow waveguide transitions (See Fig. 8(a)) are employed at the 16 output ports to achieve the matching to the LSGs [27]. With the optimized dimensions shown in Fig. 8, a reflection coefficient of lower than -20 dB and all the transmission coefficients within -12 ±0.05 dB are realized over the entire operating bandwidth, which exhibit a good input impedance matching and output amplitude balance.

It is important to note that when more radiation slots are required, the proposed feeding structure only needs to expand horizontally without increasing its vertical profile. This extremely useful feature contributes to the compactness and low-profile of the proposed CTS array.
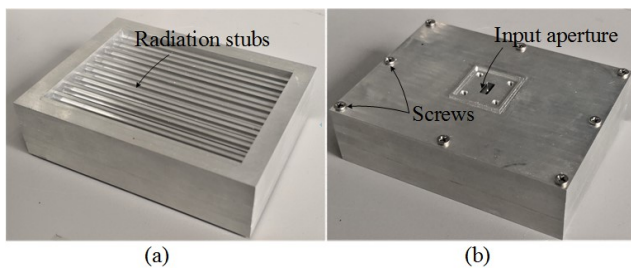

Fig. 10. Photographs of ARRAY-I: (a) View from the radiation side; (b) View from the feeding side.

E. Experimental results

ARRAY-I has been prototyped using aluminum blocks. During assembly, a set of screws are placed around the antenna for tightening to suppress wave leakage. The photographs of the assembled CTS array are shown in Fig. 10. The antenna array is 78.8 mm × 54.6 mm × 21 mm in size. Its radiation performance was measured using near-field vertical planar scanner systems from NSI-MI Technologies. The reflection coefficient was measured using Agilent E8361C network analyzer.
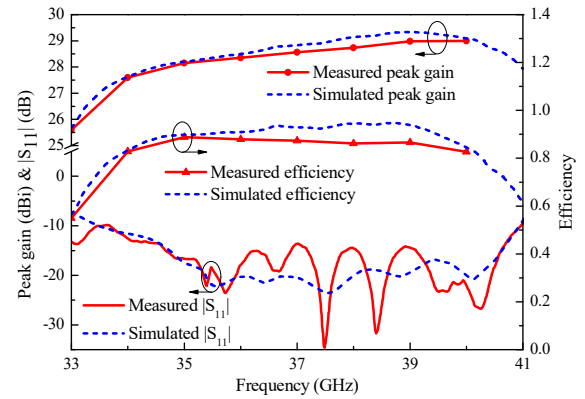
1) Reflection coefficient, gain and efficiency

Fig. 11. Simulated and measured reflection coefficients, peak gain and aperture efficiency.

Shown in Fig. 11 are the reflection coefficient, peak gain and aperture efficiency. The measures reflection coefficient is better than -13 dB between 34 and 41 GHz and in good agreement with simulations.

At the center frequency of 37 GHz, the peak gain is 28.6 dBi and the aperture efficiency is 87.3%. With the help of the high-efficiency LSGs, a constant and high aperture efficiency of over 83% is achieved across the bandwidth of 34 - 41 GHz. The measured peak gain is in the range of 27.6 – 29.0 dBi, slightly lower than the simulated. The small difference (~0.4 dB) is believed to be mainly from the fabrication and assembling tolerance and measurement error.

2) Radiation patterns

The simulated and measured normalized radiation patterns in the E- and H-planes at 34, 37 and 40 GHz are presented in Fig. 12. Again, a very good agreement is obtained between the simulated and measured results, where the patterns almost superimpose. The E-plane patterns are controlled by the uniform amplitude distribution imposed on the different radiating slots. The side lobe levels (SLLs) in the E-plane patterns are below -13 dB. The H-plane patterns are determined by the quasi-TEM wave generated by the LSGs. The achieved SLLs are also around -13 dB. The 3-dB beamwidths at the center frequency are 7.6° and 5.4° for E-plane and H-plane, respectively. Beyond ±40° in the H-plane, there are some small differences between simulation and measurement, which can be attributed to assembly error between the linear source generator and the radiation layer. This would have resulted in an uneven energy distribution in the H-plane. The measured cross-polarization patterns are also plotted in Fig. 12. The cross-polarization level is below -35 dB for both planes.

3) Comparisons with other work

Table I compares the performance of this design with two other published CTS antenna arrays. All the works utilized

This article has been accepted for publication in a future issue of this journal, but has not been fully edited. Content may change prior to final publication. Citation information: DOI 10.1109/TAP.2018.2883574, IEEE Transactions on Antennas and Propagation

> REPLACE THIS LINE WITH YOUR PAPER IDENTIFICATION NUMBER (DOUBLE-CLICK HERE TO EDIT) <   6
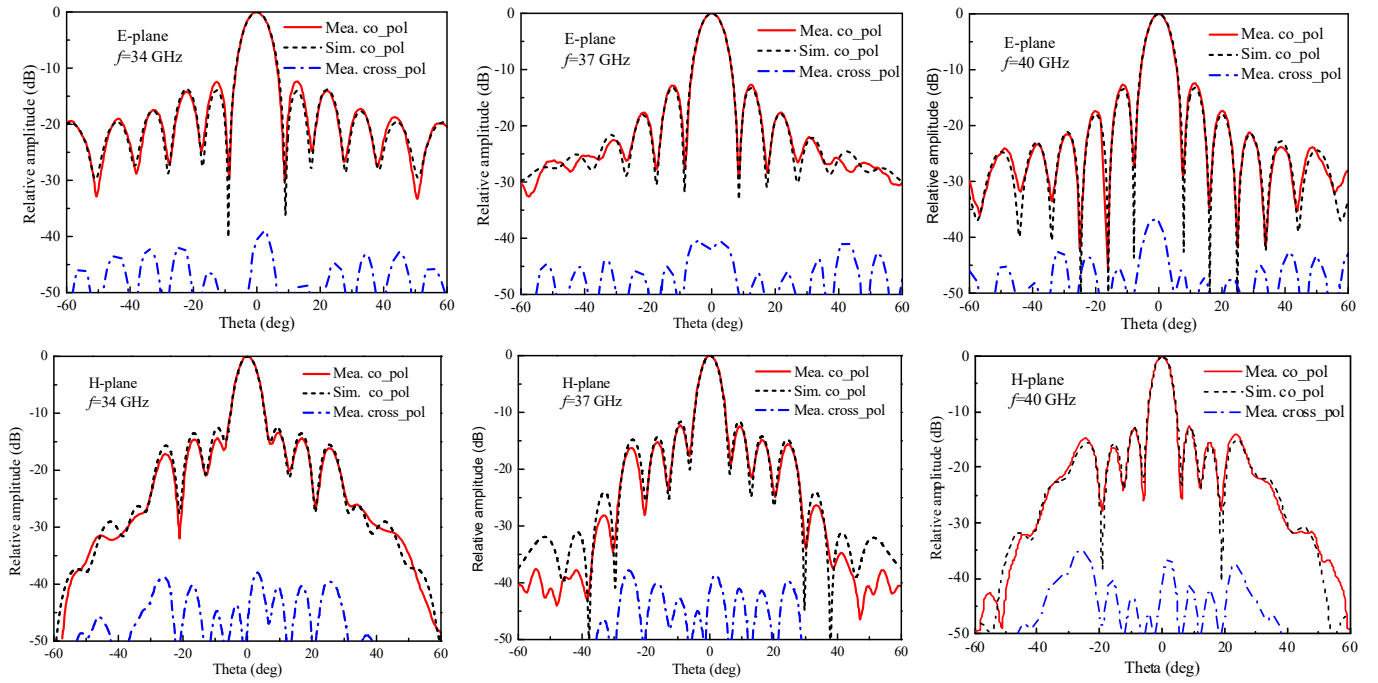

Fig.12. Normalized radiation patterns in E-plane and H-plane at 34, 37 and 40 GHz.

metal waveguides. In the previous work, due to the non-uniform distribution of the excitations generated by the pillbox couplers, the peak gains and radiation efficiencies were compromised. With the new LSG, the CTS antenna array shown here offers a significant improvement in the aperture efficiency and profile while maintaining a good or at least comparable impedance bandwidth and other radiation performance.

TABLE I
PERFORMANCE COMPARISON OF WAVEGUIDE-BASED CTS ANTENNA ARRAY

Ref.	Slots no.	Impedance Bandwidth	Peak gain (dBi)	Efficiency	Profile size $(\lambda_0^3)^*$
[19]	32	n.a.	28.2	n.a. (8 GHz)	n.a.
[21]	32	>19%	30.8	48% (73 GHz)	43.2 × 25.1 × 8.8
This work	8	>18.7%	28.6	87.3% (37 GHz)	9.72 × 6.74 × 2.5

$^*\lambda_0$ is the free space wavelength at the center operating frequency.

IV. DESIGN AND ANALYSIS OF ARRAY-II

Now we will present the second CTS array with a LSG structure but using substrate integrated waveguide (SIW) technology. The main design drive here is to minimize the number of substrate layers by using the LSGs. The concerned frequency band is from 24.5 GHz to 29.5 GHz with a center frequency f_{c2} of 27 GHz. All the substrates used have ε_r = 2.94 and $\tan\delta$ = 0.0015.

A. SIW Antenna configuration

The configuration of the SIW-based CTS array (Array-II) is shown in Fig. 13(a). There are two main differences (key features as well) in the antenna architecture as compared with the waveguide array (Array-I). One is the use of the superstrate matching layer (Layer M1) for the radiators. The other less

obvious but more fundamental difference is in the LSG structure. Array-I has a partial-corporate feed whereas Array-II has a full-corporate feed. The series feeding part as in the cavity sections 2 and 2' shown in Fig. 1 is eliminated. As a result, the phase imbalance due to the series feed is avoided and no extra phase compensation structure is needed. The length of the LSG unit is halved accordingly. Elsewhere the SIW array architecture is similar to Array-I. It contains four substrate layers with different thickness, namely substrate #1, #2, #3 and #4.

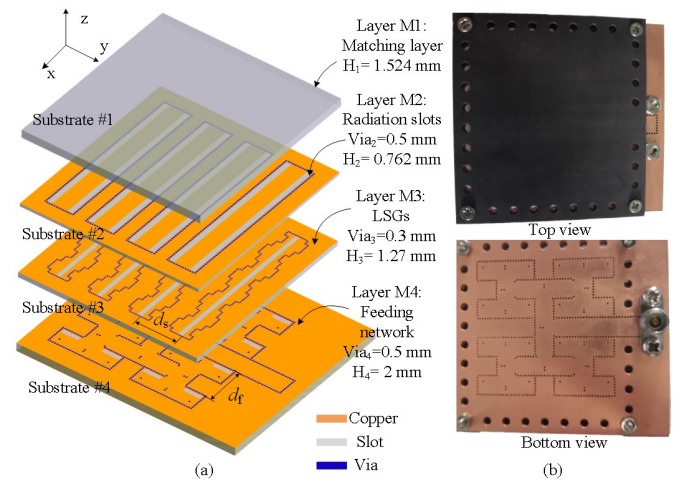
Fig. 13. Array-II based on SIW: (a) Configuration; (b) Photographs.

B. Feed network

A planar single-substrate 16-way power divider is employed to feed the LSG, as shown in Fig. 14. It consists of four H-shape power dividers. Each one contains three T-junctions. A short row of two metalized vias are positioned at the junction for impedance matching. One metal via is added by each aperture

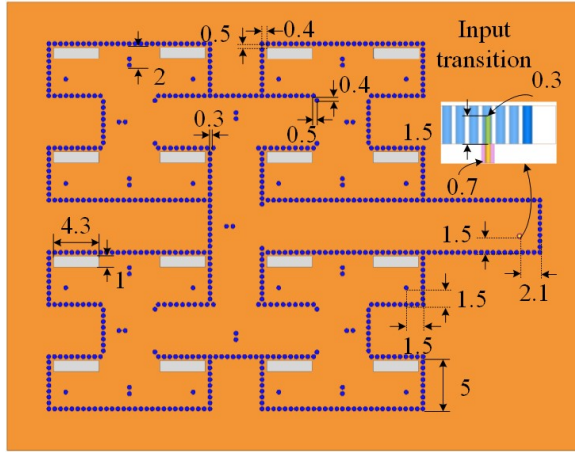to improve the output impedance matching [28].

Fig. 14. Top view of the feed network. All dimensions are given in millimeters.

A probe transition is employed between the input connector and the SIW structure. With the optimized dimensions shown in Fig. 14, the feed network achieves reflection coefficient below -15 dB over the band of 24.5-29.5 GHz and a balanced transmission coefficient within -12.3 ± 0.3 dB across the sixteen output apertures.
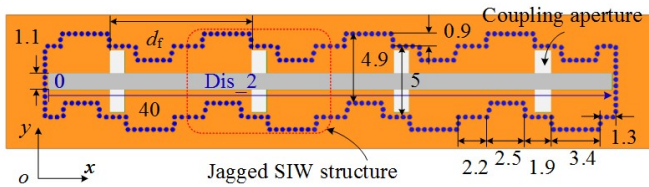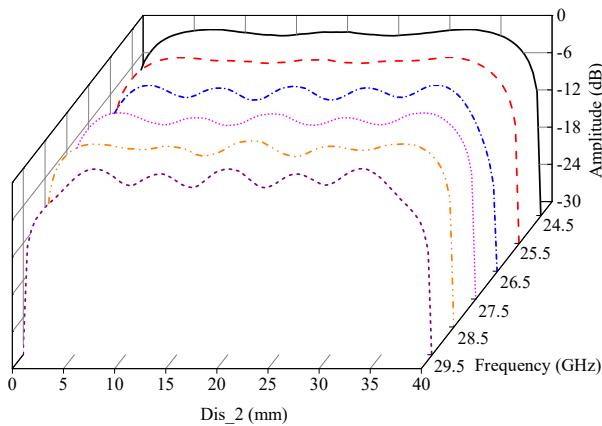

Fig. 15. The LSG structure in ARRAY-II.

Fig. 16. E-field amplitude distribution along the slot of the LSG.

C. Linear source generator

Fig. 15 shows one of the four LSGs. Each is fed by four coupling apertures with a unit length d_f (~λ_{gmin}. In Array-I, the unit length is ~$2\lambda_{gmin}$), which is set to be 10 mm. The total length of the radiation slot is 40 mm. Fig. 16 shows the amplitude distribution of E-field along the output slot (labeled with 'Dis_2' in Fig. 15). The amplitude fluctuation is lower

than 3 dB.

D. Radiation part

The eight radiation slots are divided into four groups, each excited by one LSG. An E-plane SIW-based PPW junction is achieved in substrate #2, as shown in Fig. 13(a). The distance d_s between the adjacent radiation slots is chosen to be 0.85 λ_{gmin}, so that no grating lobes occurs over the entire bandwidth.
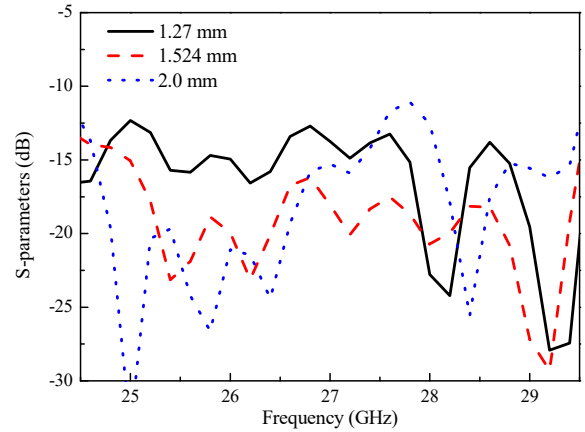
Fig. 17. Effect of the thickness of the superstrate on impedance matching.

The superstrate #1 on top of the radiation slots is used to improve the impedance matching [22]. Fig. 17 shows the simulated reflection coefficients under different superstrate thickness. When the thickness is 1.524 mm, a reflection coefficient lower than -15 dB can be achieved over the bandwidth of 24 - 30 GHz.
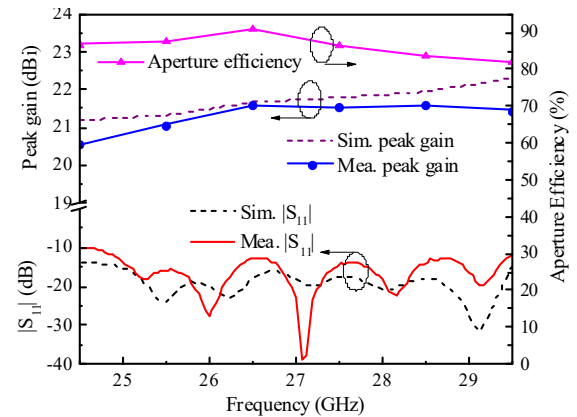
Fig. 18. Simulated and measured reflection coefficients, peak gain and aperture efficiency.

E. Experimental results

Array-II has been prototyped using printed circuits board (PCB) technology. A set of screws are used around the antenna to press the substrates together. Conductive silver paste is used between substrates to suppress wave leakage. The photographs of the assembled antenna array are shown in Fig. 13(b). The antenna array is 40 mm × 37 mm × 5.86 mm in size. The radiation performances are measured using MVG compact-range antenna test system.

Fig. 19. Normalized radiation patterns of the SIW CTS array in E-plane and H-plane at 24.5, 27 and 29.5 GHz.

The simulated and measured reflection coefficients, peak gains and aperture efficiency are shown in Fig. 18. Reasonably good agreement has been achieved. Th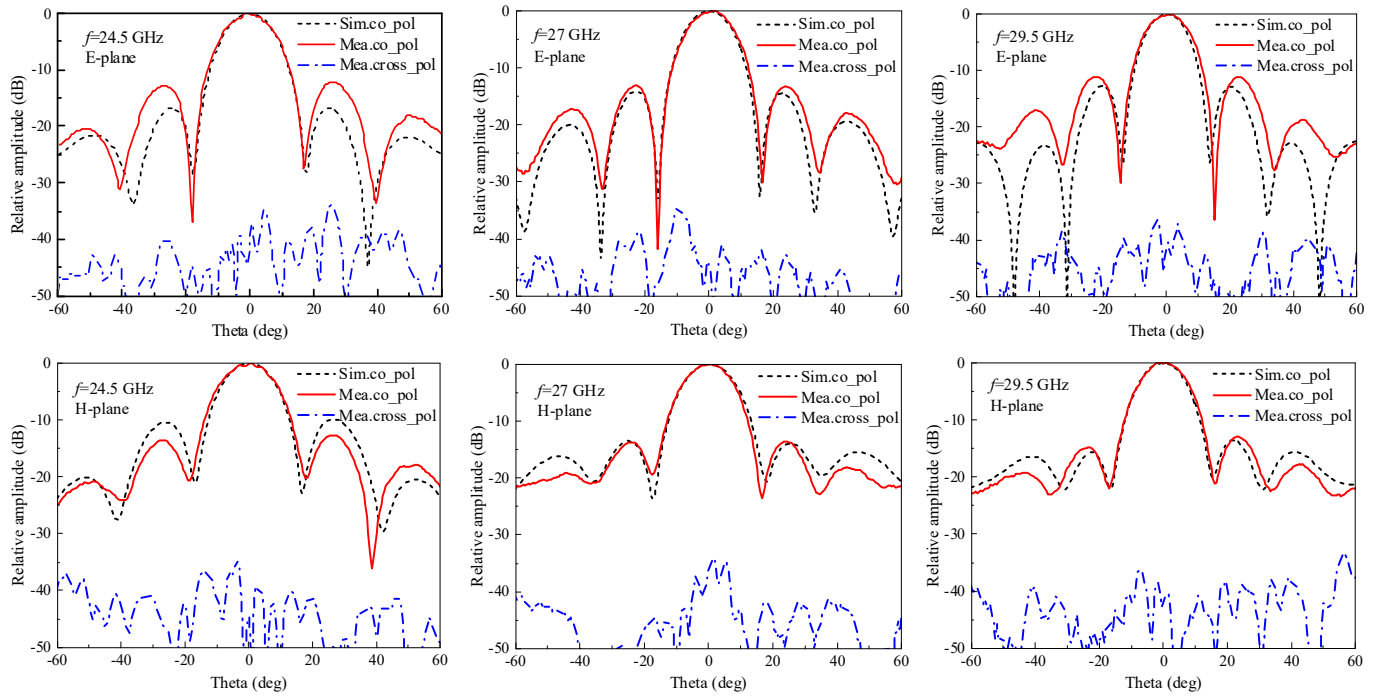e matching is better than -10 dB over 24.5- 29.5 GHz. The simulated peak gain is in the range of 21.2 – 22.3 dBi, whereas the measured is 20.6 – 21.6 dBi. At the center frequency of 27 GHz, the peak gain is 21.5 dBi and the aperture efficiency is 88.2%. Again, the constant and high aperture efficiency of more than 82% is attributed to the uniform quasi-TEM wave generated by the LSG.

TABLE II
PERFORMANCE COMPARISON OF MULTIPLAYER CTS ANTENNA ARRAYS

Ref.	Type	No. Slots	Total layers	Impedance bandwidth	Efficiency	Peak gain (dBi)
[22]	LTCC	4	18	>25.2%	44% (60 GHz)	14.3
This work	SIW	8	4	>18.2%	>82%	>20.6

The normalized radiation patterns in the E- and H-planes at 24.5, 27 and 29.5 GHz are presented in Fig. 19. A very good agreement is obtained between the simulated and measured. The small discrepancy is partly caused by the measurement error and partly by the imperfection in fabrication and assembly. The E-plane 3-dB beamwidth at the center frequency is 13.8° as defined by the uniform amplitude distribution over the different radiating slots. The H-plane 3-dB beamwidth at the center frequency is 15.6° as defined by the quasi-TEM wave generated by the LSGs. Over the operating bandwidth, the measured first SLL is below -12.2 dB / -12.7 dB in the E- and H-planes, respectively. The measured cross-polarization patterns, plotted in Fig. 19, are below -32 dB for both planes.

There is very little previous work on CTS arrays using multi-layer PCB technology. Table II compares with one other published CTS array based on LTCC [22]. Only four radiation slots were implemented using 18 LTCC layers. The peak gain and aperture efficiency were much lower than those of this work. The low efficiency is believed to be mainly from the pillbox LSG structure. Our SIW array achieves higher performance using only four substrate layers.

V. CONCLUSION

In this paper we demonstrated a novel linear source generator structure utilized in two CTS antenna arrays demonstrating high efficiency with a low profile. The multi-layer PPW network and pillbox structures, widely used in many CTS arrays, have been replaced with compact corporate-feeds and the LSG with jagged cavity structures. The high efficiency of the antenna is attributed to a uniform amplitude and phase excitation from the LSG. Two demonstrators were presented using two different technologies: hollow-waveguide (Array-I) and SIW (Array-II). The experimental results show that the two arrays realized 18.7%/18.5% impedance bandwidth with a peak gain of better than 27.6 dBi/20.6 dBi, respectively. The aperture efficiencies of both prototypes are higher than 82% over the entire band. Very good agreement between measurement and simulation has been achieved. The low-profile and high performance of the proposed CTS antenna is well suited for millimeter-wave 5G and point-to-point communication links. It may also find usefulness in emerging applications such as vehicle radars and communications.

REFERENCES

[1] M. Dyadyuk, J. D. Bunton, and J.P.Athikulangara, "A multigigabit millimeter-wave communication system with improved spectral efficiency," *IEEE Trans. Microw. Theory Tech.*, vol. 55, no. 12, pp. 2813–2821, Dec. 2007.

This article has been accepted for publication in a future issue of this journal, but has not been fully edited. Content may change prior to final publication. Citation information: DOI 10.1109/TAP.2018.2883574, IEEE Transactions on Antennas and Propagation

> REPLACE THIS LINE WITH YOUR PAPER IDENTIFICATION NUMBER (DOUBLE-CLICK HERE TO EDIT) <   9

[2] I. Papageorgiou, A. Derneryd, L. Manholm, and J. Yang, "An E-band cylindrical reflector antenna for wireless communication systems," in *Proc. Eur.Conf. AntennasPropag. (EuCAP)*, pp. 524–528, Apr. 2013.

[3] E. B. Lima, J. R. Costa, and C. A. Fernandes, "Broadband reflector fed by integrated lens antenna with frequency constant directivity," in *IEEE Antennas Propag. Soc. Int. Symp.*, 2010, pp. 1–4.

[4] M. Al-Nuaimi, W. Hong, and Y. Zhang, "Design of high directivity compact size conical horn lens antenna," *IEEE Antennas Wireless Propag. Lett.*, vol. 13, pp. 467–470, Jan. 2014.

[5] Y. Miura, J. Hirokawa, M. Ando and Y. Shibuya, "Double-layer Full-corporate-feed hollow-waveguide slot array antenna in the 60-GHz Band," *IEEE Trans. Antennas Propag.*, vol. 59, no. 8, pp. 2844–2851, Jun. 2011.

[6] M. Zhang, J. Hirokawa, and M. Ando, "An E-band partially corporate feed uniform slot array with laminated quasi double-layer waveguide and virtual PMC terminations," *IEEE Trans. Antennas Propag.*, vol. 59, no. 5, pp. 1521–1527, May. 2011.

[7] N. Ghassemi and K. Wu, "High-efficient patch antenna array for E-band gigabyte point-to-point wireless services," *IEEE Antennas Wireless Propag. Lett.*, vol. 11, pp. 1261–1264, Oct. 2012.

[8] A. E. I. Lamminen, J. Säily, and A. R. Vimpari, "60-GHz patch antennas and arrays on LTCC with embedded-cavity substrates," *IEEE Trans. Antennas Propag.*, vol. 56, no. 9, pp. 2865–2874, Sep. 2008.

[9] B. Zhang and Y. P. Zhang, "Grid array antennas with subarrays and multiple feeds for 60-GHz radios," *IEEE Trans. Antennas Propag.*, vol. 60, no. 5, pp. 2270–2275, May 2012.

[10] J. R. James, P. S. Hall, and C. Wood, Microstrip Antenna: Theory and Design, Belgium: Peter Peregrinus, 1981.

[11] Y. J. Cheng, Y. X. Gui, and Z. G. Liu, "W-band large-scale high-gain planar integrated antenna array," *IEEE Trans. Antennas Propag.*, vol. 62, no. 6, pp. 3370–3373, Jun. 2014.

[12] Y. She, R. Fujino, J. Hirokawa, M. Ando, D. Hanatani, and M. Fujimoto, "LTCC oversized rectangular waveguide slot array antenna with air-layer in the radiating part in the millimeter-wave band," *IEEE Trans. Antennas Propag.*, vol. 61, no. 4, pp. 1777–1783, Apr. 2013.

[13] Y. Tyagi, P. Mevada, S. Chakrabarty, R. Jyoti "High-efficiency broadband slotted waveguide array antenna," *IET Microw. Antennas Propag.*, vol. 11, no. 10, pp. 1401–1408, Aug. 2017.

[14] G. L. Huang, S. G. Zhou, T. H. hio, H. T. Hui, and T. S. Yeo, "A low profile and low sidelobe wideband slot antenna array feb by an amplitude-tapering waveguide feed-network" *IEEE Trans. Antennas Propag.*, vol. 53, no. 1, pp. 419–423, Jan. 2015.

[15] W.W.Milroy, "Continuous transverse stub (CTS) element devices and methods ofmaking same," U.S. patent 5,266,961,Aug. 1991.

[16] W. W. Milroy, "Compact, ultrawide-band antenna feed architecture comprising a multistage, multilevel network of constant reflectioncoefficient components," U.S. Patent 6 075 494, Jun. 2000.

[17] W. W. Milroy, "The continuous transverse stub (CTS) array: basic theory, experiment, and application," in *Proc. Antenna Appl. Symp.*, 1991, pp. 253–283.

[18] N. E. Lindenbald and P. Jefferson, "Multiple slot antenna," U.S. Patent 2 628 311, Feb. 1953.

[19] Y. Xu, H. Dong, Y. Liu and P. Zhang, "Continuous transverse stub (CTS) array antenna," in *Int. Symp. Antennas Propag. (ISAP)*, 2012, pp. 1083–1086.

[20] M. Ettorre, F. Foglia Manzillo, M. Casaletti, R. Sauleau, L. Le Coq, and N. Capet, "Continuous transverse stub array for Ka-band applications," *IEEE Trans. Antennas Propag.*, vol. 63, no. 9, pp. 4798–4800, Sep. 2015.

[21] T. Potelon, M. Ettorre, L. L. Coq, T. Bateman, J. Francey, D.Lelaidier, E. Seguenot, F. Devillers and R. Sauleau, "A low-profile broadband 32-slot continuous transverse stub array for backhaul applications in E-band," *IEEE Trans. Antennas Propag.*, vol. 65, no. 12, pp. 6307–6316, Dec. 2017.

[22] F. F. Manzillo, M. Ettorre, M. S. Lahti, K. T. Kautio, D. Lelaidier, E. Seguenot and R. Sauleau, "A multilayer LTCC solution for integrating 5G access point antenna modules," *IEEE Trans. Microw. Theory Tech.*, vol. 64, no. 7, pp. 2272–2283, Jun. 2016.

[23] K. Tekkouk, J. Hirokawa, R. Sauleau, and M. Ando, "Wideband and large coverage continuous beam steering antenna in the 60-GHz band", *IEEE Trans. Antennas Propag.*, vol. 65, no. 9, pp. 4418–4426,Sep. 2017.

[24] Q. C. You, Y. L. Lu, G. M. Xu, and J. F. Huang, "Design of a 4 × 4 Low Profile Continuous Transverse Stub Antenna Array," Progress In Electromagnetics Research Symposium-Fall (PIERS- FALL), Singapore, 19–22 November 2017, pp. 1465-1469

[25] F. F. Manzillo, M. Ettorre, M. Casaletti, N. Capet, and R. Sauleau, "Active impedance of infinite parallel-fed continuous transverse stub arrays," *IEEE Trans. Antennas Propag.*,vol. 63, no. 7, pp. 3291–3297, Jul. 2015

[26] M. Ando, Y. Tsunemitsu, M. Zhang, J. Hirokawa and S. Fujii, "Reduction of long line effects in single-layer slotted waveguide arrays with an embedded partially corporate Feed," *IEEE Trans. Antennas Propag.*, vol. 58, no. 7, pp. 2275–2280, Mar. 2010.

[27] R.Vincenti Gatti; R. Rossi, "Wideband compact single-ridge waveguide to rectangular waveguide transitions with integrated E-plane bend," *Electron. Lett.*, vol. 52, no. 20, pp. 1699–1701, Sep. 2016.

[28] Q. Zhu, K. B. Ng, C. H. Chan and K. Luk, "Substrate-integrated-waveguide-fed array antenna covering 57–71 GHz band for 5G applications," *IEEE Trans. Antennas Propag.*, vol. 65, no. 12, pp. 6298-6306, Dec. 2017.